N. C. Blais and D. G. Truhlar,
in *Potential Energy Surfaces and Dynamics Calculations*,
edited by D. G. Truhlar (Plenum Press, New York, 1981),
pp. 431-473.

REACTION, DISSOCIATION, AND ENERGY TRANSFER AS A FUNCTION OF INITIAL STATE FOR H + H_2 ON AN ACCURATE *AB INITIO* POTENTIAL ENERGY SURFACE

Normand C. Blais

University of California
Los Alamos Scientific Laboratory
Los Alamos, NM 87545

Donald G. Truhlar

Department of Chemistry
University of Minnesota
Minneapolis, MN 55455

I. INTRODUCTION

We present here the results of quasiclassical trajectory calculations for H + H_2 collisions. Our emphasis is to examine the dependence of the energy transfer, dissociation, and atom-exchange processes on the initial internal state of the H_2 molecule, including states of high internal energy. For these high-energy states the transition probabilities are large and the concern with zero point energy is minimized; these conditions help justify our use of quasiclassical trajectories for the dynamical calculations. In the present study we use an accurate potential energy surface[1-3] so that the calculations are more realistic than is possible for other systems for which the uncertainties in the potential energy surface are much greater.

All of the work we are reporting pertains to the state-to-state reactions

$$H_A + H_BH_C(v,j) \rightarrow H_A + H_BH_C(v',j') \quad \text{(R1)}$$

$$\rightarrow H_{AB}(v',j') + H_C \text{ or } H_AH_C(v',j') + H_B \quad \text{(R2)}$$

$$\rightarrow H_A + H_B + H_C \quad \text{(R3)}$$

where v and j are initial vibrational and rotational quantum numbers and primes denote final (postcollision) values. Although H + H_2 is a very widely studied system,[4,5] most previous work has been directed to $v \leq 1$ and low j. In the present study, we consider v from 0 to 12 and j from 0 to 30.

II. CALCULATIONAL PROCEDURES

The potential energy surface representing the H_3 interatomic forces is the one of Liu, Siegbahn, one of the present authors, and Horowitz (LSTH). It is a functional representation[1] to accurate *ab initio* points calculated by Liu[2] for collinear geometries and by Siegbahn and Liu[3] for other geometries. The LSTH surface has been used by others in quantum mechanical calculations,[6,7] semiclassical calculations,[8] and quasiclassical calculations,[9,10] but the highest energy state of H_2 included in those studies was $v = 1, j = 0$.[10] Of special concern to us in this work is the fact that the LSTH potential reduces exactly to the Kolos-Wolniewicz potential[11] for H_2 upon removing the third H atom. This allows a realistic treatment of highly excited states of H_2. Our characterization of the initial and final molecular energy states is based on the methods we reported earlier[12] for the Ar + H_2 system and corresponds closely to the true hydrogen system.

Most of the details of the trajectory calculations are the same as described previously.[12,13] All of the calculations are quasiclassical, *i.e.*, the vibrational and rotational action variables are restricted to have the correct quantized values at the start of the collision but, except for this and the final-state analysis after the collision, the internuclear motion is purely classical under the influence of the quantum mechanical potential energy surface.[14] The only initial states considered were para-hydrogen states, *i.e.*, states with even rotational quantum numbers. As will be indicated, some runs are for a given initial vibration-rotation state while other runs are for vibration-rotation states selected by Monte Carlo methods from the distribution of quantized states that has the desired temperature. Similarly, the relative translational energy is sometimes fixed for a run while for other runs a random selection is made from a predetermined distribution characteristic of a temperature. In the latter case importance sampling[15] is sometimes used to improve the convergence of the calculated quantities such as the

rate constant and activation energy for the exchange reaction. Thus, rather than selecting the initial relative translational energy from a Maxwell-Boltzmann distribution, we use a distribution that has been modified from a Maxwell-Boltzmann distribution by the importance sampling function of Muckerman and Faist. This causes a larger fraction of the selected collision energies to lie at higher, more reactive values. Each trajectory is then weighted[15] to account for the biased selection.

Final-state quantum numbers v' and j' are assigned by either the histogram or the smooth sampling method.[12] For nonexchange collisions the final-state rotational quantum number j' is assigned an even value to conserve parity. For exchange collisions, j' is assigned as either even or odd. The total rate for producing odd j' states is the rate of para-to-ortho conversion. For state-to-state results we prefer here to state the distinguishable-atom exchange cross sections and rate constants rather than the para-to-ortho ones.

At times, when a trajectory ends up in a state very near the boundary between the bound and quasibound states, the final rotational quantum number assigned by our usual rules is not consistent with the category into which the trajectory is placed by other considerations, *i.e.*, bound for negative internal energy or quasibound for positive internal energy. In such cases, we alter our rules for the rotational quantum number assignment and change the integer value by one level spacing to make the assignment consistent. The rotational action variable, which is used for computing classical final-state averages, is not changed.

For calculations corresponding to a fixed relative translational energy (E_{rel}) we calculate cross sections and their error estimates (all error estimates are at the 68% confidence level) using the methods of reference 12. For very highly excited initial states with a thermal distribution of E_{rel}, we used unweighted Monte Carlo sampling and calculated rate constants, average cross sections,[16] and Tolman activation energies[14,16-19] by the methods of references 12 and 16. For other calculations involving thermal distributions of E_{rel}, we use importance sampling as discussed above. The importance sampling function is[15]

$$P_r^0(E_{rel}) = \frac{1}{m!}\left(\frac{E_{rel}}{kT}\right)^{m-1} \tag{1}$$

where m is assigned an appropriate value in the range 2-11, depending on initial state and temperature. In these cases the rate constants and their error estimates are calculated by equations (21) and (22) of reference 15, the effective cross sections and their error estimates are calculated from the rate quantitites by equation (36) of reference 12, the average cross sections and their error estimates

are calculated from the rate quantities by equation (6) of reference 16, and the Tolman energies of activation are calculated by equations (2)-(8) in section IV of this paper.

The fixed-E_{rel} calculations reported here are based on 40,877 trajectories, the state-selected calculations with 300 K and 1000 K distributions of E_{rel} are based on 13,767 and 1818 trajectories, respectively, and the completely thermal calculations at 444 K, 875 K, and 2400 K are based on 25,715 trajectories. All of the trajectory calculations were done on a Digital Equipment Corporation VAX 11/780 computer in double precision. The initial and final conditions for each trajectory, including coordinates and momenta, were stored on disk for future reference.

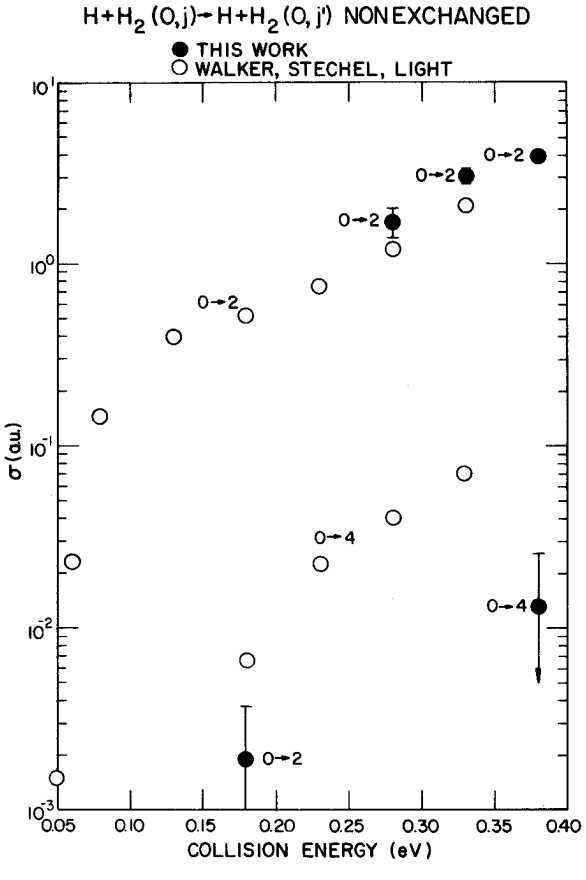

Fig. 1. Nonreactive rotational excitation cross sections (in a_0^2) for $H + H_2(0,j) \rightarrow H + H_2(0,j')$ as a function of relative translational energy. The results in this figure are based on 1040, 386, 600, and 1000 trajectories at the four energies respectively.

III. COMPARISON WITH OTHER WORK

Several of the runs were carried out expressly to make comparisons with other work, either quantum mechanical calculations or quasiclassical trajectories. These runs are generally for low-internal-energy states of H_2, whereas the major part of the work reported here is for high-internal-energy states. Nevertheless, some interesting comparisons can be made and we can also make checks for consistency. For the results presented in this section, the final states of the trajectories were assigned by the histogram method.[12]

Figure 1 shows the cross sections we obtain for nonreactive energy transfer involving transitions from $H_2(v=0,j=0)$ to $H_2(v=0,j'=2,4)$ as a function of relative translational energy. On the same graph we have plotted the results of Walker *et al.*[20] for the same LSTH potential. Their calculations are three-dimensional quantal close coupling calculations, including four vibration states and a total of 40 channels in the basis set. Our quasiclassical results show a much higher threshold than do the quantum results for both the $j = 0$ to $j' = 2$ and the $j = 0$ to $j' = 4$ transitions. The quasiclassical cross sections for the $0 \rightarrow 2$ transition also have a much stronger energy dependence near threshold than do the quantum results, but the agreement is good at energies well above threshold.

Green and one of the present authors[7] calculated j-to-j' transition rates for H + H_2 quantum mechanically in the rigid-rotator approximation using the LSTH potential. For comparison, Fig. 2 shows the present calculations of the j-to-j' cross sections for $v = 0$ at two different temperatures, 444 K and 875 K. (Note: Figure 2 was calculated by sorting trajectories from the completely thermal runs that are discussed in section IV below.) We present the results of both sets of calculations in Fig. 2 as thermally averaged effective cross sections. This quantity[16] is the thermally averaged cross section for those collisions with energy above the energetic threshold for reaction, *i.e.*, we have divided the thermally averaged cross sections by the fraction of collisions with enough total energy to cause the quantal state-to-state transition so that the dynamical aspects of the cross section are more apparent. At 875 K our results are almost always higher by a considerable factor as compared to the quantal rigid-rotator ones. At 444 K the agreement is not really any better, but there is no consistent trend between the two sets of points. The only reasonably good agreement is for the $0 \rightarrow 2$ and $2 \rightarrow 0$ transitions at 444 K. The poor correlation between the two sets of calculations must be caused by the rigid-rotator assumption in the quantal calculations, the classical approximations in the present calculations, or both. Walker and Stechel[21] have shown that the rigid-rotator approximation leads to an underestimate of the rotational excitation cross section for H + H_2 on the LSTH surface. This explains the direction of the difference of the 875 K results in

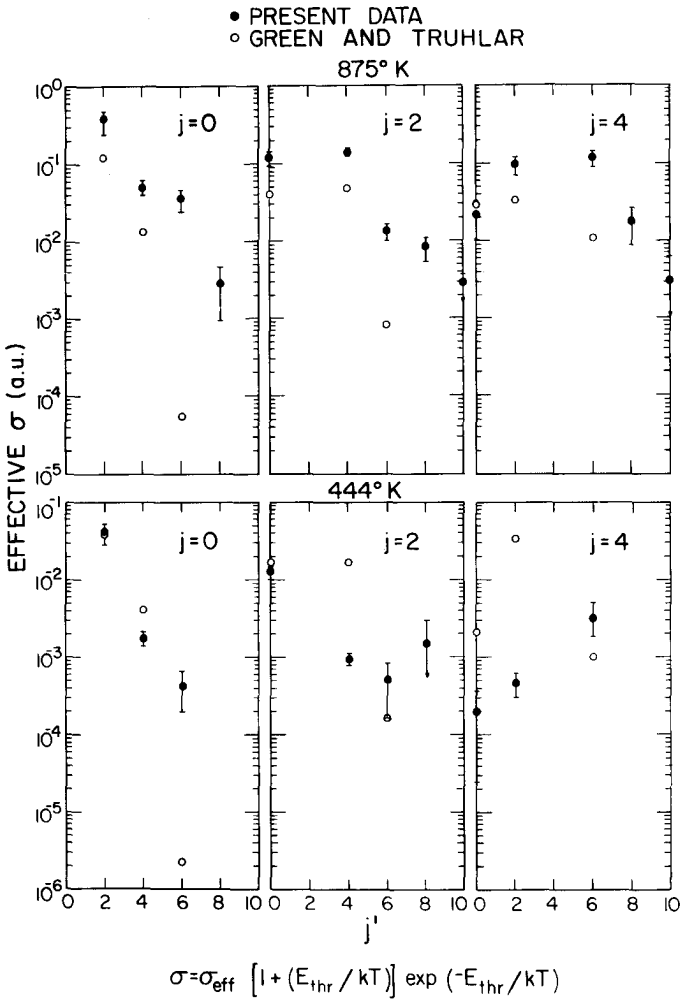

Fig. 2. Thermally averaged effective cross sections (in a_0^2) for $H + H_2(0,j) \rightarrow H + H_2(0,j')$ as functions of j'. The cross sections are averaged over a thermal distribution of relative translational energy at 444 K and 875 K. The Green-Truhlar results are rigid-rotator calculations, but the present calculations include vibrational motion. The arrow at the lower limit of one of the error bars indicates our uncertainty as to that lower limit. If only one trajectory contributed to the cross section we defined the uncertainty to be 100%.

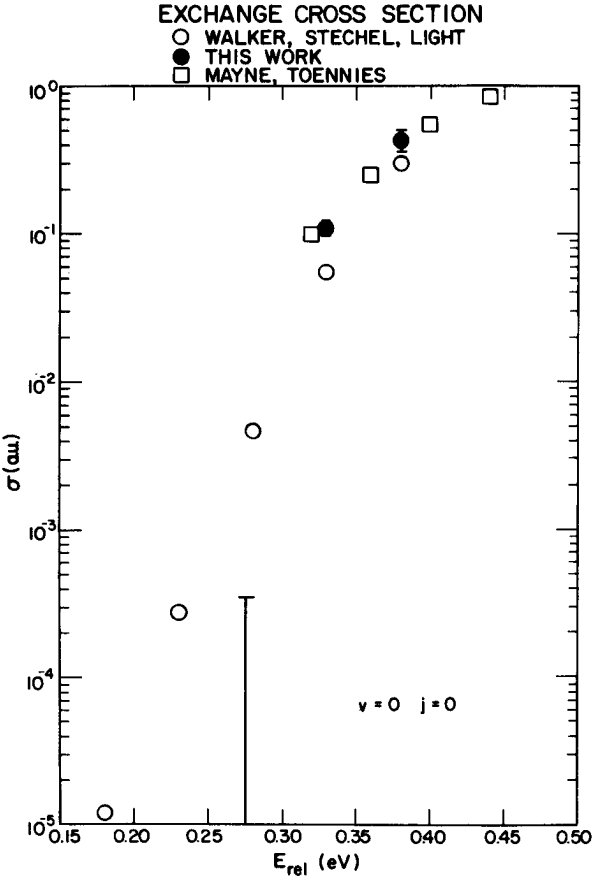

Fig. 3. The cross section (in a_0^2) for the exchange reaction (R2) with v = 0,j = 0, as a function of relative translational energy. The top of the error bar at 0.28 eV indicates what the trajectory result would have been if one trajectory had reacted. The results at 0.28 eV and 0.33 eV are based on 800 and 1633 trajectories, respectively, with smaller maximum impact parameters than the batches used for Fig. 1. The results at 0.38 eV are based on the same 1000 trajectories as used for Fig. 1.

Fig. 2. Apparently, the threshold errors of the quasiclassical calculations illustrated in Fig. 1 are more important at 444 K, and they compensate the rigid-rotator errors enough to even change the direction of the difference for some transitions. The trajectory calculations should be most reliable at high temperature. Some additional inelastic cross sections are presented in section VI where they are compared to reactive state-to-state cross sections.

We can also compare our reaction cross sections for $v = 0, j = 0$ with other sets of results. One is a quantal calculation by Walker *et al.*[6] which is similar in many respects to those of reference 20. The other data are from quasiclassical trajectory calculations by Mayne and Toennies.[9] Again, all of the calculations use the LSTH potential; the results are shown in Fig. 3. To search for the threshold we made special runs for $E_{rel} = 0.28$ eV, one with a very small impact parameter, $0.3\ a_0$; the top of the error bar at that energy in Fig. 3 indicates the value that would have been calculated for the cross section if only one of the trajectories had reacted. The classical threshold is therefore very close to 0.28 eV, and the energy dependence of the cross section near threshold is clearly different than that predicted by quantum mechanics. The two trajectory calculations agree well with each other, and they both agree with the quantum results at a relative translational energy of 0.33 eV and above.

The cross sections in Fig. 3 may be partitioned into state-to-state cross sections for specified final states. This is done in Table 1. At 0.33 eV there is little excitation of product rotation; but at 0.38 eV, the trajectories predict appreciable excitation of $j' = 1$ and 2. For comparison Table 1 also gives the thermally averaged state-to-state cross sections for $v = 0, j = 2$ with a 300 K distribution of relative translational energies; these cross sections were calculated from trajectories discussed in section V. Under thermal conditions the reaction is more rotationally adiabatic than for the fixed-energy cases in Table 1 even though the average value of E_{rel} for reactive collisions in the thermal case is 0.411 eV.

For comparison with previous work, we also carried out calculations with $v = 1, j = 2$, and a 300 K distribution of relative translational energy. The state-to-state rates for both reactive and nonreactive processes were summed over j' to yield the $v \to v'$ partially state-selected rates in Table 2. These rates are generally consistent with other theoretical work but not with the available experiments. Since this work is discussed (with appropriate references) in the overview chapter by Schatz in this book, we will not discuss it here.

An internal consistency check of our trajectories can be made by looking at how well detailed balance is preserved. Trajectories run with completely thermal intiial conditions, *i.e.*, with the

Table 1
Cross sections (in Å^2) for the reaction H + H_2(v=0,j=0) → H_2 + H(v',j').[a]

final state v',j'	j = 0 E_{rel} = 0.33 eV	j = 0 E_{rel} = 0.38 eV	j = 2 E_{rel} @ 300 K
0,0	0.021	0.039	b
0,1	0.010	0.046	2.0×10^{-7}
0,2	b	0.035	1.3×10^{-6}
0,3	b	0.004	1.4×10^{-7}
0,4	b	b	5.6×10^{-8}
0,5	b	b	4.5×10^{-8}
0,6	b	b	3.7×10^{-10}

a. all cross sections in this table were calculated by the histogram method

b. no trajectories observed in these bins

Table 2
Rate constants for processes with specified initial and final vibrational numbers at 300 K relative translational temperature.[a]

Process	j	v	v'	k(cm^3 molecule^{-1} s^{-1})
Reactive	2	1	0	2.2×10^{-14}
Nonreactive	2	1	0	9.4×10^{-15}
Total	2	1	0	3.2×10^{-14}
Reactive	2	1	1	4.3×10^{-14}
Reactive	2	1	all	6.5×10^{-14}

a. rates are summed over j', and v' is assigned by the histogram method

Table 3
A check for detailed balance. The ratio of $k(j \to j')/k(j' \to j)$ for nonreactive collisions with $v = v' = 0$ is tabulated. The distribution of relative translational energies is thermal at 444 K and at 875 K.

j	j' = 2	j' = 4	j' = 6	j' = 8
		T = 444 K		
0	2.2 ± 0.8 (1.6)[a]	0.98 ± 0.89 (0.20)		
2		0.53 ± 0.19 (0.13)		
4			0.027 ± 0.027 (0.061)	
		T = 875 K		
0	2.8 ± 0.9 (2.8)	1.0 ± 0.6 (1.3)	0.2 ± 0.2 (0.38)	
2		0.9 ± 0.35 (0.47)	0.06 ± 0.05 (0.14)	0.03 ± 0.03 (0.008)
4			0.5 ± 0.2 (0.29)	

a. the values in parentheses are exact values calculated from $(2j' + 1)/(2j + 1) \exp\{-[E_{int}(v=0,j') - E_{int}(v=0,j)]/kT\}$

internal energy of the H_2 molecule and the relative translational energy both selected from appropriate thermal distributions, were sorted out to make up Table 3. The completely thermal runs are discuseed further in section IV below. The ratios $k(0,j \to 0,j')/k'(0,j' \to 0,j)$ and their error estimates are given in Table 3 for two different temperatures, 444 K and 875 K. The exact ratio is shown in parentheses and was calculated from the expression at the bottom of the table. In the first two rows and columns, where the error bars are reasonably small, detailed balance is preserved. Even where the error bars are large, the predicted ratios fall within the uncertainties of the trajectory ratios.

IV. THERMAL RATE CONSTANTS AT 444-2400 K

We made completely thermally averaged runs to obtain well converged values for the thermal rate constant k_r and the activation energy E_a for the atom exchange reaction (R2). For this purpose we calculated 4892 trajectories with m = 9 [see equation (1)] for 444 K, 4818 trajectories with m = 7 for 875 K, and 16,005 trajectories with m = 7 for 2400 K. The first two temperatures were chosen because experimental results are available for comparison at these temperatures, and the latter was chosen to compare to transition-state-theory calculations at high temperature. Care was taken that a sufficiently large value of the maximum impact parameter b_{max} was used to ensure good convergence of the results. The values used for the three temperatures were 2 a_0 for 444 K, 2.25 a_0 for 875 K, and 2.8 a_0 for 2400 K.

Table 4 shows the results for the rate constant. The column indicated by ‡ is for a three-dimensional transition-state-theory calculation[22] using the LSTH potential. Transition-state-theory results corrected for tunneling are indicated by ‡/MCPVAG, which means that the transmission coefficients were calculated using the Marcus-Coltrin path and the vibrationally adiabatic ground-state potential curve, as explained elsewhere.[23] The other columns list the experimental data[25-28] with which we wish to compare. The numbers in square brackets are extrapolations from lower temperature experiments. The comparison to experiment is satisfactory, considering the probable errors in the older data[27,28] and the discrepancies between the newer results.[25,26] At low T, the quasiclassical trajectory rate constant is less than $k^{‡/MCPVAG}(T)$ due to neglect of tunneling, and it is greater than $k^{‡}(T)$ due to "nonadiabatic leak".[14] At high T the transition-state-theory calculations predict too high a rate, probably due to recrossing effects.[29,30] The quasiclassical trajectory rate constants therefore lie below the $k^{‡/MCPVAG}(T)$ at all three temperatures.

The Arrhenius activation energy was calculated using the Tolman derivation:[14,16-19]

$$E_a = \langle E_{rel} + E_{int} \rangle_{reactions} - \langle E_{rel} + E_{int} \rangle_{collisions} + \frac{1}{2}kT \tag{2}$$

$$= E_{a,rel} + E_{a,int} \tag{3}$$

where

$$E_{a,rel} = \langle E_{rel} \rangle_{reactions} - \frac{3}{2}kT \tag{4}$$

Table 4
Rate constants for $H + H_2 \rightarrow H_2 + H$.[a]

T(K)	k_r(cm^3 $molecule^{-1}$ s^{-1})						
	trajectories	‡	‡/MCPVAG	SLeR[b]	QLeR & WdeH[c]	Farkas[d]	van Meersche[e]
444	6.7 ± .8(-15)	3.42(-15)	9.49(-15)	7.7(-15)	1.0(-14)		
875	8.0 ± .7(-13)	6.47(-13)	8.99(-13)	[4.4(-13)][f]	[9.9(-13)][g]	2.5(-12)	3.1(-12)
2400	3.5 ± .3(-11)	4.50(-11)	4.63(-11)				

a. numbers in parentheses are powers of ten

b. Schulz and LeRoy, reference 24

c. Quickert and LeRoy, reference 25, for $k(H + H_2)/k(H + D_2)$ combined with Westenberg and N. DeHaas, reference 26, for $k(H + D_2)$

d. from 1930 paper (reference 27), probably unreliable

e. from 1951 paper (reference 28), probably unreliable

f. extrapolated from 404-444 K. Extrapolation from 300-444 K yields 1.5(-12). Therefore, extrapolation is unreliable.

g. extrapolated from $k(H + H_2)/k(H + D_2)$ at 294-693 K and $k(H + D_2)$ at 549-745 K

and

$$E_{a,int} = \langle E_{int} \rangle_{reactions} - \langle E_{int} \rangle_{collisions} \tag{5}$$

where E_{int} is the internal energy of the reagents and the averages are over all reactions in the ensemble or all collisions in the ensemble. The averages over reactions were computed by[19]

$$\langle E_{rel} \rangle_{reactions} = \sum_{i=1}^{N_r} w_i E_{rel,i} \Big/ \sum_{i=1}^{N_r} w_i \tag{6}$$

and

$$\langle E_{int} \rangle_{reactions} = \sum_{i=1}^{N_r} w_i E_{int,i} \Big/ \sum_{i=1}^{N_r} w_i \tag{7}$$

where N_r is the number of reactive trajectories and w_i, $E_{rel,i}$, and $E_{int,i}$ are the weight, relative translational energy, and internal energy of trajectory i. The quantity $\langle E_{int} \rangle_{collisions}$ was computed from the reactant energy levels $E_{v,j}$ by

$$\langle E_{int} \rangle_{collisions} = \sum_{v,j} (2j+1) E_{v,j} e^{-E_{v,j}/kT} \Big/ \sum_{v,j} (2j+1) \times e^{-E_{v,j}/kT} \tag{8}$$

In principle, $\langle E_{int} \rangle_{collisions}$ could also be computed by a formula like (7) by including all trajectories rather than just reactive ones; in practice since m is chosen to improve the sampling of reactive initial conditions, the importance sampling can lead to slow convergence of quantities involving all collisions. Thus equation (8) is preferred.

Table 5 gives the results for the total energy of activation, for which we compare our results with those from the same sources as in Table 4. All of the calculations show an activation energy which increases with increasing temperature. An Arrhenius plot of the logarithm of the rate of reaction *versus* (1/T) would therefore not be a straight line but would be concave upward. Notice that the temperature dependence of E_a is much greater than is usually assumed. Large temperature dependences of E_a have also been observed in previous theoretical work when a large enough temperature range was studied.[31-33] Table 6 gives the breakdown of the activation energy calculations into a relative translational contribution and an internal energy contribution. At the two lower temperatures there are only small populations of the significantly excited states of the reactants; then the average value of the internal energy is

Table 5
Energies of activation for $H + H_2 \rightarrow H_2 + H$.

T(K)	E_a (eV)				
	trajectories	‡	‡/MCPVAG	SLeR	QleR & WdeH
444	0.34 ± .01	0.40[a]	0.33[a]	0.350[b]	0.327[c]
875	0.38 ± .01	0.43[d]	0.39[d]		(0.358)[e]
2400	0.60 ± .09	0.63[f]	0.62[g]		

a. 400-500 K

b. from non-Arrhenius fit of 300-444 K data. Using just the data at 404-444 K yields 0.336 eV.

c. from data at 346 and 549 K. Using data at 440 and 549 K yields 0.400 eV.

d. 720-1000 K

e. from data at two highest temperatures, 549 K and 720 K

f. 1500-4000 K

g. 1500-4000 K (‡/MCPSAG)

Table 6
Components of the activation energy (in eV) computed by the quasiclassical trajectory method.

T(K)	reactions		collisions		$E_{a,rel}$	$E_{a,int}$	E_a
	$\langle E_{rel} \rangle$	$\langle E_{int} \rangle^a$	$\frac{3}{2}kT$	$\langle E_{int} \rangle^a$			
444	0.41	-4.45	0.06	-4.44	0.35	-0.01	0.34
875	0.50	-4.41	0.11	-4.40	0.39	-0.01	0.38
2400	0.81	-4.11	0.31	-4.21	0.50	0.11	0.60

a. zero of energy for E_{int} is dissociated molecule, *i.e.*, atoms

within 0.1 eV of the ground-state value of -4.48 eV. At 2400 K the excited states play a greater role; the activation energy apparently increases because all the excitation energy is not available for overcoming the barrier. Thus, the excited molecular states have greater total energy requirements for reaction and the average energy of reactive collisions increases more rapidly than the average energy of all collisions.

The trajectory results for the activation energy are lower than the transition-state-theory ones at all temperatures. But the agreement becomes noticeably better if the tunneling correction is included in transition state theory. Because the classical trajectories don't include tunneling, this improved agreement must be fortuitous. A preliminary communication of the activation energy calculations is given elsewhere.[34]

V. STATE-SELECTED RATE CONSTANTS AT 300 K

We were especially interested in seeing how several reaction attributes changed as the initial H_2 state was changed over the manifold of bound states. So we performed a series of calculations for which the distribution of relative translational energies was thermal at a temperature of 300 K, but the initial molecular quantum numbers were varied over a wide range. In fact, the present study includes a wider range of variation of the initial state than any previous dynamical calculations on any system except perhaps for our own studies of[12,16]

$$Ar + H_2(v,j) \rightarrow Ar + H + H \qquad (R4)$$

In Fig. 4 we plot k_r *versus* the initial internal energy of H_2. The quantum numbers v,j are indicated next to the error limits for each point. The upper set of points all correspond to j = 2, and the internal energy increases because of an increase in v. The lower set represents v = 0, and the energy increases because of an increase in j. Clearly for a given internal energy, vibration is much more effective for exchange than rotation. In fact, the ratio of the rates for the (v,j=2) and (v=0,j) states with similar energies is at least a factor of 10 and sometimes 10^2 or 10^3. However, one should not assume that rotation is ineffective in promoting reaction. The v = 6,j = 20 state has nearly the same energy difference from the 0,20 state and the 6,2 state so that it may be thought of as having nearly equal vibrational and rotational energies. Yet it has a reaction rate that is about four times higher than the 6,2 state. And the 0,20 state has reaction rate 10^5 times larger than the 0,2 state. Another interesting comparison involves the 0,14; 3,2; 0,22; and 6,2 states. The former two have excitation energies with respect to the ground state of 1.34 and 1.50 eV respectively, whereas the latter two

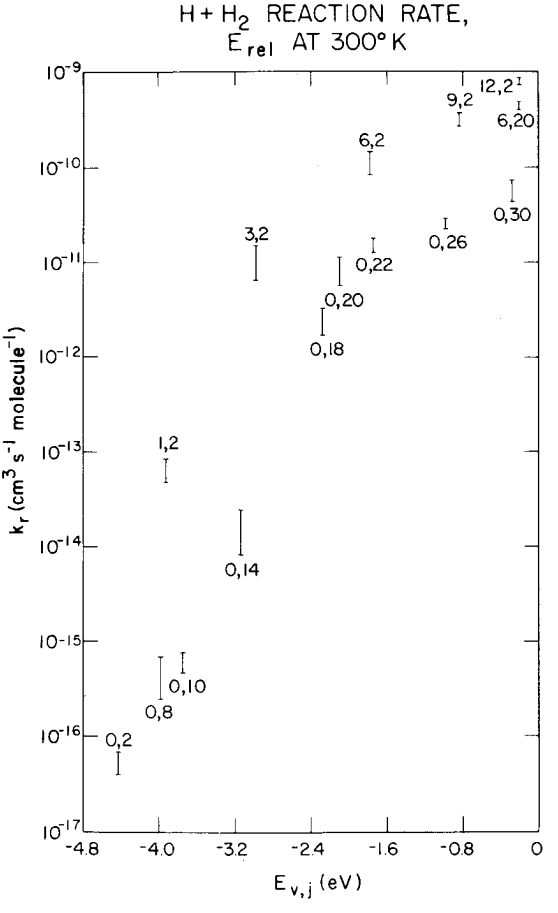

Fig. 4. The rate constant (in cm^3 $molecule^{-1}$ s^{-1}) for the exchange reaction (R2) at 300 K as a function of the initial molecular internal energy. The quasiclassical quantum numbers for the initial states are indicated next to the entries for the state-selected rate constant.

have excitation energies of 2.75 and 2.70 eV, respectively. Yet the rate increases by a factor of 860 when 0,14 is excited to 0,22, but only by a factor of 11 when 3,2 is excited to 6,2.

The systematics of the state-selected reactions at 300 K are illustrated in more detail in nine of the next ten figures. Figure 5 shows the rate constant for even more initial states than are included in Fig. 4; and Figs. 6-9 show additional quantities that

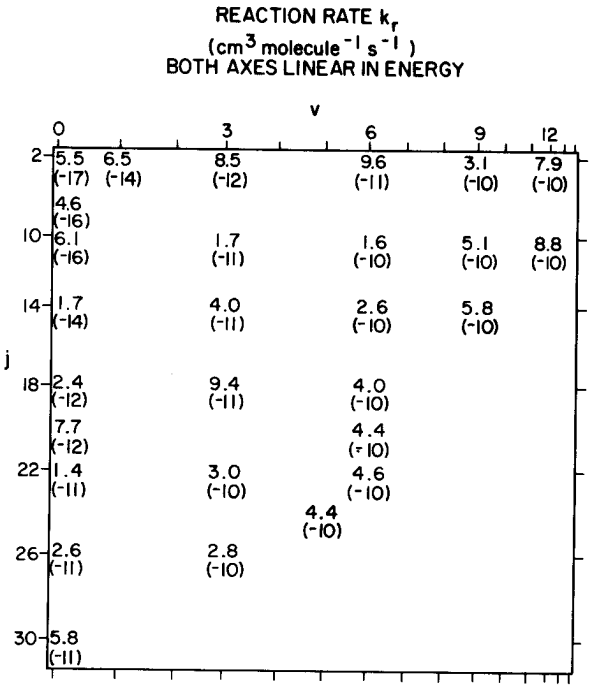

Fig. 5. The rate constant (in cm^3 $molecule^{-1}$ s^{-1}) for the exchange reaction (R2) for various initial states for a 300 K distribution of relative translational energy. Numbers in parentheses are powers of 10. The initial vibrational and rotational quantum numbers are indicated on the abscissa and ordinate respectively. The abscissa is chosen to be linear in energy for (v,0) states, and the ordinate scale is chosen to be linear in energy for (0,j) states.

characterize the final states of these initial-state-selected reactions. In order to show how these quantities depend on the initial molecular state, one axis is marked off with initial vibrational quantum number and the other with the initial rotational quantum number. The scales of the axes are both linear in energy for states with pure vibrational excitation or pure rotational excitation so that the energy dependence of the quantity being plotted is more evident. However, since vibration and rotation energies are not additive, the energy-linearity of the scale is strictly true only on the axes.

Closely associated with the reaction rate is the activation energy, which is shown in Fig. 6. Looking along both axes, we see that the activation energy decreases with an increase in v or j but that the decrease is much more dramatic with v than with j. The

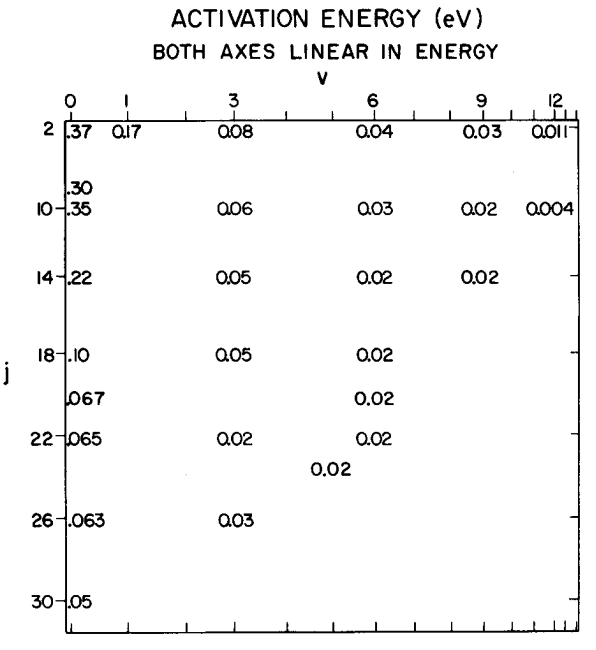

Fig. 6. The activation energy (in eV) for the exchange reaction (R2) for various initial states for a 300 K distribution of relative translational energy. The axes are as in Fig. 5.

reaction rate dependence on v and j shown in Figs. 4 and 5 can be accounted for mostly by this trend in the activation energy. The trend for vibration to be more effective than rotation for causing the exchange reaction is also evident for states that are close to the dissociation limit, which corresponds in the plot to a line running roughly diagonal from $v = 0, j = 30$ to $v = 14, j = 0$.

In Fig. 7 we show the average final vibrational quantum number of the exchange product. The tendency for adiabaticity of the vibrational mode during exchange is very evident in this figure. In fact, for initial states with $j = 10$, the vibrational quantum number changes very little from reactant to product. But, as might be expected intuitively, at high initial j, $R \rightarrow V$ energy transfer during exchange becomes an important factor. Similarly, at low initial j, $V \rightarrow R$ energy transfer is clearly discernible.

The average final rotational quantum number is shown in Fig. 8. In marked contrast to vibration, the rotational mode does not have a tendency to be very adiabatic. Only at very low j (from 2 to less than 10) and low v does j' have the same average value as j. At

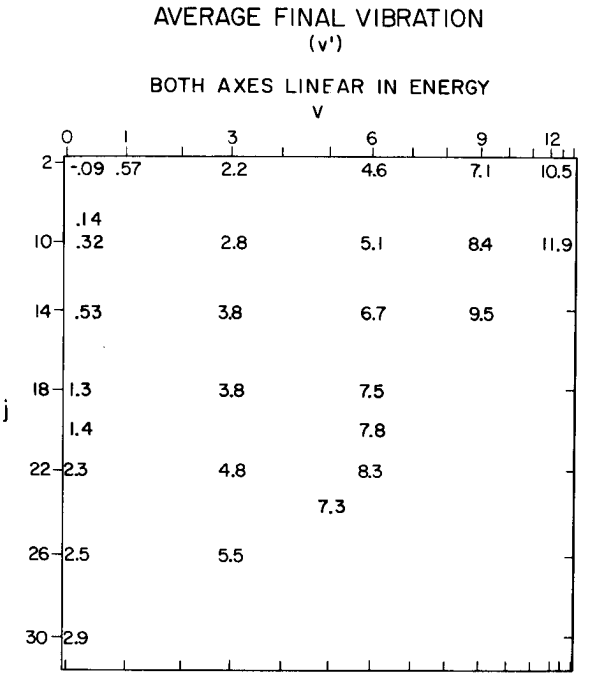

Fig. 7. The average final vibrational quantum number for the exchange product of reaction (R2) for various initial states for a 300 K distribution of relative translational energy. The quantity given is $\langle v' \rangle$, where $(v' + \frac{1}{2})h = J'_v$, where J'_v is the final vibrational radial action variable. The axes are as in Fig. 5.

$j = 2$ and higher v the V→R energy transfer discussed in connection with Fig. 6 is evident. For $j \geq 8$ there is a net energy loss from rotation. Because vibration does not change very much during exchange, the energy lost from rotation appears mainly as translation. Therefore, for exchange at high internal energies, the products are translationally hotter than the reagents.

In connection with Figs. 7 and 8, it is interesting to consider the experiments of Blackwell, Polanyi, and Sloan.[35] They demonstrated experimentally that vibration is nearly adiabatic in the almost thermoneutral reaction Cl + OH → HCl + O. By using two different prereactions, they were able to product OH radicals with two different vibrational distribuions to use as reagents in a second reaction with Cl. For one set of conditions, the reaction was predominantly with the $v = 1$ and 2 levels of OH, and for the other with $v = 6$ through 9. The product HCl was found to be mainly in levels $v' = 1$ and 2 for the first case and in $v' = 9$ and 10 for the other. Because of the slightly

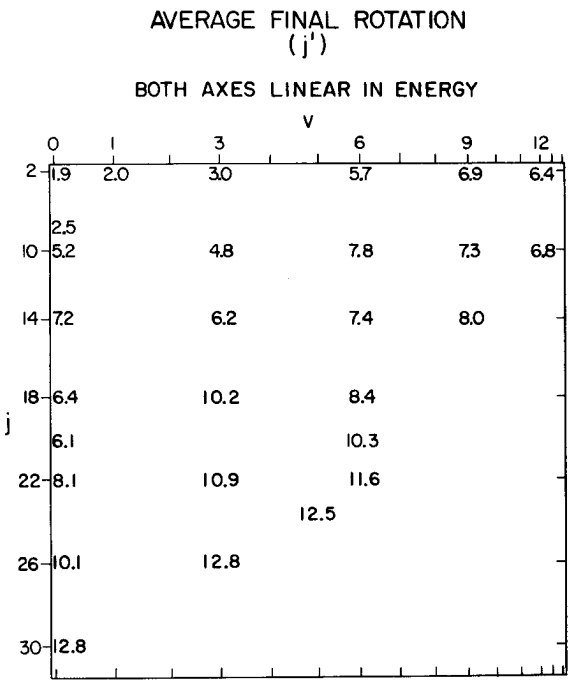

Fig. 8. The average final rotational quantum number for the exchange product of reaction (R2) for various initial states for a 300 K distribution of relative translational energy. The quantity given is $\langle j' \rangle$ where $(j' + \frac{1}{2})h = J_\theta/2\pi = J'_\theta$, where J'_θ is the final rotational action variable and J' is the final rotational angular momentum. The axes are as in Fig. 5.

different level spacing of HCl as compared to OH this means that there was actually a slight dimunition in vibrational energy from reactant to product. The initial average j was not very high under either conditions and their results indicate an increase in the average rotational quantum number and rotational energy during the reaction. Our calculations for low initial j are in good qualitative agreement with the experimental evidence. For high initial j, where there is no experimental evidence available, our calculations predict that the role of rotation may become quite different.

The molecular scattering angle accompanying the exchange reaction is shown in Fig. 9. The angle is measured with respect to the initial direction of motion of the atom. For scattering angle, rotation and vibration seem to play similar roles. For either kind of excitation the scattering angle decreases with increasing energy. Rotation may be slightly more effective. It has long been recognized

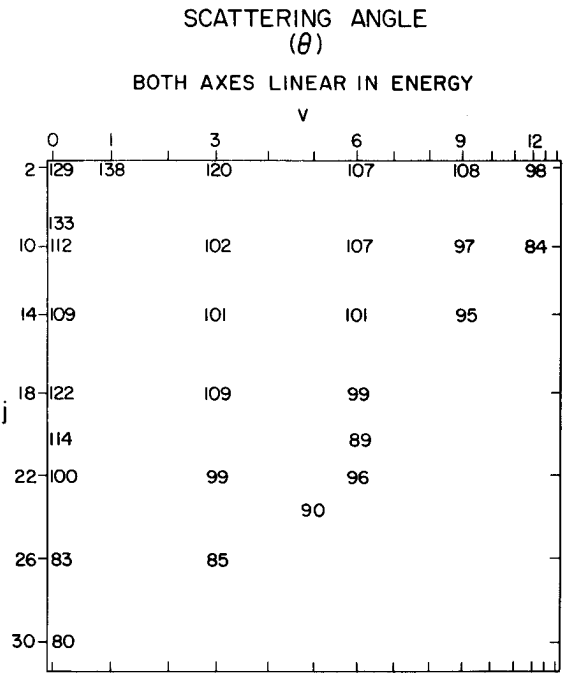

Fig. 9. The average final scattering angle for the exchange product of reaction (R2) for various initial states for a 300 K distribution of relative translational energy. The axes are as in Fig. 5.

that a large reaction cross section implies forward-dominated scattering, while a small cross section often means backward scattering.[36] This generalization is, of course, mitigated by extreme mass combinations of reagents or by the type of potential energy surface or energy release during the reaction.[37] But we are changing none of these by changing the internal energy. Therefore, the trend to scatter forward with increasing cross section is well illustrated in Fig. 9. Clearly though, the role of the initial angular momentum has a separate importance, as already seen by the disparity between the cross sections at high v and those at high j. One must be cautious in drawing very detailed conclusions because of the slow convergence sometimes manifested in Monte Carlo calculations; nevertheless, it is interesting to notice the apparent structure in the dependence of average scattering angle on increasing j at $j \tilde{=} 18$. Perhaps this should be investigated further.

As already discussed, Fig. 7 shows how the average final vibrational state changes when the initial state is changed. It is of interest to see the distributions that lead to those averages. In

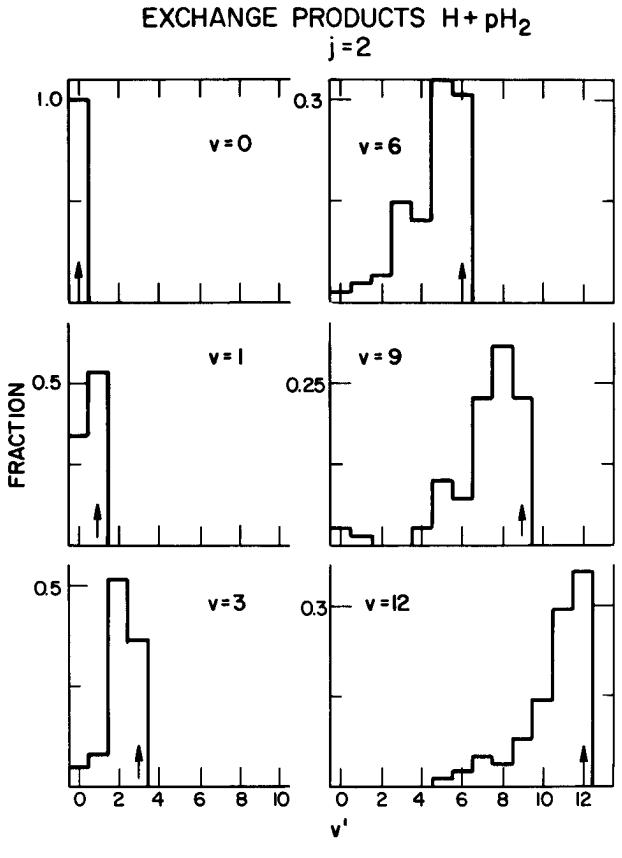

Fig. 10. Distributions of final vibrational quantum number v' for the exchange product of reaction (R2) as functions of v. The ordinate is the fraction in the final state v'. Each distribution is labelled by the initial vibrational quantum number v, which is further indicated by an arrow. The initial rotational quantum number j is 2, and the initial relative translational energy corresponds to a 300 K distribution.

Figs. 10, 11, and 12, we show the distribution of final vibrational quantum number for each of the initial vibrational states that were examined at j = 2, 10, and 18. These distributions were computed by the histogram method. They show that for each j, as v increases, the distribution in v' broadens to about a width of 6 or 7 states; this seems to be the maximum breadth of the distribution. The average value of v' then changes relative to v with increasing j by shifting the peak to a higher value of v'. More quantitative information about the widths of the v' and j' distributions is given in Table 7, where the root-mean-square widths of these

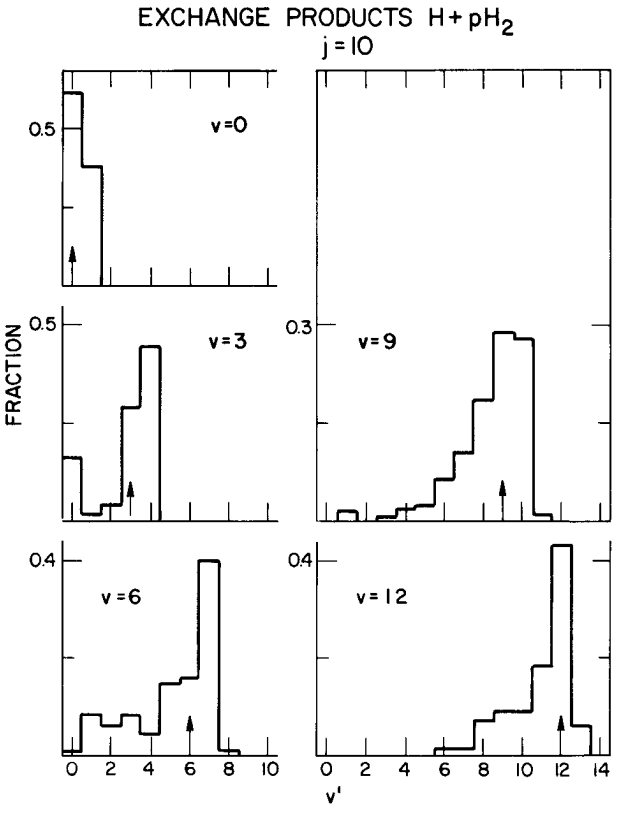

Fig. 11. Same as Fig. 10 except j is 10.

distributions are tabulated. In general both rms widths increase as reactant internal energy increases, but this is only a general trend; there are many exceptions.

Table 7 also illustrates the average changes in molecular internal energy. For low-j,v = 0 reactions, the average product internal energy is actually less than the zero-point energy. This is similar to what is sometimes observed in v = 0 nonreactive collisions at low energy;[38] in both cases the systems tend to transfer some of their zero-point energy into translation in low-energy collisions. In every case in Table 7, the molecular internal energy decreases on the average in reactive collisions. This is probably a consequence of the low translational temperature as compared to the high internal energy of the molecules as measured with respect to their classical minimum energy. Thus, the tendency of the trajectories toward classical equilibration leads to a net transfer of internal energy into translational energy. In some cases the effect

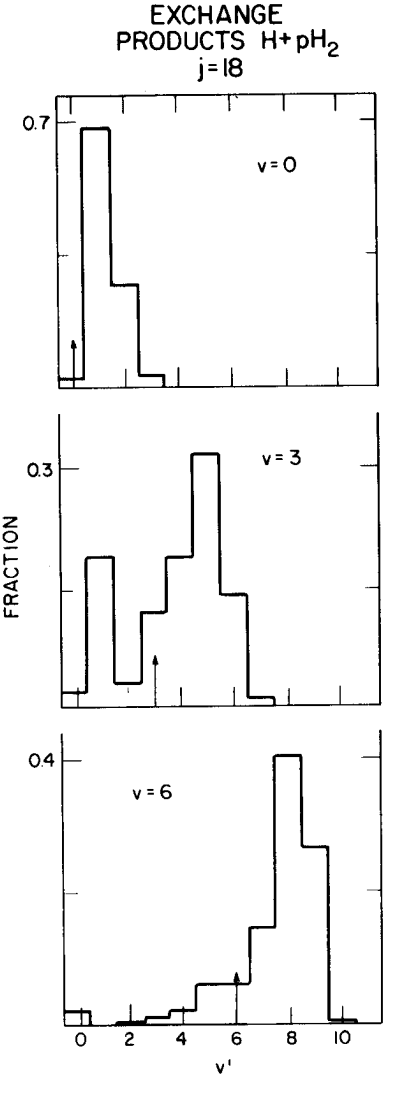

Fig. 12. Same as Fig. 10 except j is 18.

Table 7
Reactant internal energies and three averages over reaction products for state-selected reactions at 300 K.

state v,j	$E_{int}(v,j)^a$ (eV)	$\langle E'_{int} \rangle^a$ (eV)	$\langle (v' - \langle v' \rangle)^2 \rangle^{1/2}$	$\langle (j' - \langle j' \rangle)^2 \rangle^{1/2}$
0,2	-4.43	-4.48	0.11	0.71
0,8	-3.97	-4.32	0.20	1.32
0,10	-3.73	-4.04	0.39	2.46
0,14	-3.14	-3.77	0.15	2.31
0,18	-2.46	-3.46	0.52	2.64
0,20	-2.09	-3.45	0.77	2.24
0,22	-1.73	-2.84	0.86	3.15
0,26	-0.99	-2.54	1.37	3.61
0,30	-0.28	-2.07	1.43	2.46
1,2	-3.92	-4.13	0.35	1.24
3,2	-2.98	-3.28	0.66	1.68
3,10	-2.38	-2.91	1.37	2.50
3,14	-1.88	-2.37	1.28	3.01
3,18	-1.32	-1.98	1.57	4.63
3,22	-0.721	-1.54	1.13	4.13
3,26	-0.139	-1.15	1.96	4.59
5,24	0.030[b]	-0.644	2.17	5.13
6,2	-1.78	-2.09	1.43	3.77
6,10	-1.29	-1.71	2.05	4.71
6,14	-0.886	-1.26	1.20	3.12
6,18	-0.441	-0.937	1.72	3.95
6,20	-0.218	-0.688	1.45	4.38
6,22	-0.004	-0.470	1.94	5.13
9,2	-0.841	-1.16	1.95	4.13
9,10	-0.468	-0.767	1.77	4.05
9,14	-0.182	-0.470	1.69	3.89
12,2	-0.208	-0.333	1.64	4.09
12,10	-0.0004	-0.104	1.62	4.20

a. zero of energy is the dissociation limit. To convert zero of energy to ground state, add D_0 = 4.447 eV. To convert zero of energy to bottom of reactant potential curve, add D_e = 4.748 eV.

b. quasibound initial state

is quite dramatic, *e.g.*, the 0,26 and 0,30 states lose an average of 1.55 and 1.79 eV, respectively, in reactive collisions, and the products of the reaction of the 3,26 and 6,22 states are relatively much more strongly bound than the reactants.

The rate constants and averages in Figs. 4-9 and Table 7 all refer to bound rearranged products. Only two of the initial states considered lead to any quasibound[12] rearranged products; these are the 5,24 state, which is itself quasibound, and the 10,12 state, which is barely bound. The 5,24 state has only a small rate constant, $1.0 \pm 0.7 \times 10^{-11}$ cm^3 $molecule^{-1}$ s^{-1}, for producing rearranged quasibound products; the 12,10 state has a larger rate constant for quasibound-state production, $1.3 \pm 0.4 \times 10^{-10}$ cm^3 $molecule^{-1}$ s^{-1}, most of which corresponds to final state (12,11).

VI. ENERGY TRANSFER CROSS SECTIONS

Energy transfer from the higher energy states of a molecule is of particular importance because in the laboratory (except for a molecular beam experiment), studies of dissociation or recombination always involve a competition between the dissociation/recombination reaction and energy transfer processes. Dissociation and energy transfer processes both have large cross sections for highly excited molecules. Energy transfer is also important for laser applications.

We studied six initial states ($v = 6, j = 20$; $v = 6, j = 0$; $v = 4, j = 6$; $v = 2, j = 18$; $v = 0, j = 18$; and $v = 0, j = 6$) each with the same relative translational energy, 0.5 eV. This is just sufficient energy for a $\Delta v = +1, \Delta j = 0$ transition for five of the initial states but not for the $v = 0, j = 6$ state. A sufficiently large number of trajectories, from 3600 to 5200 depending on the initial state, was run to obtain energy transfer cross sections to nearby states with reasonably good statistical accuracy. These cross sections are given in Tables 8-12. Each table gives the results for one or two initial states. Each entry in the tables is the transition cross section and its error estimate for that final state. Most of the cross sections were computed using the smooth sampling method;[12] however, the eight final states immediately adjacent to the initial states, *i.e.*, those with $v' = v \pm 0,1$ and $j' = j \pm 0,2$ (the elastic cross sections are infinite classically and are not considered) were computed using the histogram method.[12] The reason we prefer the smooth sampling method for the general case is that for most transitions it leads to about the same cross sections as the histogram method, but it gives better convergence for a given number of trajectories. However, for nonreactive transitions to adjacent states, the smooth sampling method often leads to much larger transition probabilities, especially at large impact parameter. These larger transition probabilities are due to nearly elastic collisions for which the method

Table 8
Energy transfer cross sections (in a_0^2) for the transitions from v = 6, j = 20 to the indicated final v',j' states at 0.5 eV relative translational energy.[a,b]

j' \ v'	0	1	2	3	4	5	6	7	8	9	10	11	12	13	all v'
0	0	0.01 ±.01	0.01 ±.01	0	0	0	0	0	0	0	0	0	0	0	0.02 ±.01
2	0	0	0.01 ±.01	0.01 ±.01	0	0.01 ±.01	0	0	0	0.01 ±.01	0.01 ±.01	0.02 ±.01	0	0	0.08 ±.02
4	0	0	0	0.01 ±.01	0	0.01 ±.01	0	0	0	0.03 ±.02	0.006 ±.004	0.02 ±.02	0.01 ±.01	0.01 ±.01	0.09 ±.03
6	0	0	0	0	0	0.01 ±.01	0	0.01 ±.01	0.02 ±.01	0.02 ±.01	0	0	0.01 ±.01	0	0.08 ±.02
8	0.01 ±.01	0.04 ±.02	0.03 ±.02	0.02 ±.01	0.01 ±.01	0.05 ±.03	0.04 ±.02	0.02 ±.01	0.02 ±.01	0.02 ±.01	0.04 ±.02	0.01 ±.01	0	0	0.32 ±.06
10	0.01 ±.01	0.01 ±.01	0.01 ±.01	0.02 ±.01	0.03 ±.02	0	0.02 ±.01	0.05 ±.02	0.02 ±.01	0.02 ±.01	0.04 ±.02	0.03 ±.02	0.01 ±.01	0	0.26 ±.05
12	0	0	0	0.02 ±.01	0.02 ±.01	0	0.04 ±.02	0.10 ±.03	0.12 ±.03	0.09 ±.03	0.05 ±.02	0.01 ±.01	0		0.44 ±.07
14	0.01 ±.01	0.02 ±.02	0.01 ±.01	0.02 ±.02	0.01 ±.01	0.03 ±.02	0.05 ±.02	0.12 ±.03	0.20 ±.04	0.17 ±.04	0.01 ±.01	0			0.66 ±.08
16	0.03 ±.02	0.03 ±.02	0	0	0.02 ±.01	0.04 ±.02	0.08 ±.03	0.42 ±.06	0.55 ±.08	0.09 ±.03	0.005 ±.004	0			1.27 ±.11
18	0.03 ±.02	0.01 ±.01	0.01 ±.01	0.01 ±.01	0.06 ±.02	0.10 ±.05	0.64 ±.12	3.81 ±.30	0.32 ±.05	0					5.00 ±.33
20	0	0	0.04 ±.02	0.03 ±.01	0.15 ±.04	0.64 ±.12	...	0.43 ±.10	0.03 ±.01						1.32 ±.17
22	0.02 ±.01	0.01 ±.01	0.07 ±.03	0.08 ±.03	0.45 ±.06	4.36 ±.32	0.43 ±.10	0	0						5.43 ±.34
24	0.02 ±.01	0.03 ±.02	0.08 ±.03	0.24 ±.05	0.55 ±.08	0.28 ±.04	0	0							1.19 ±.11
26	0.01 ±.01	0.01 ±.01	0.06 ±.02	0.26 ±.06	0.09 ±.02	0	0								0.43 ±.07
28	0.01 ±.01	0.01 ±.01	0.05 ±.03	0.03 ±.01	0										0.10 ±.03
30	0.04 ±.03	0.01 ±.01	0	0											0.06 ±.03
32	0	0													0
all j'	0.19 ±.05	0.20 ±.05	0.40 ±.07	0.75 ±.09	1.38 ±.12	5.54 ±.35	1.30 ±.17	4.96 ±.32	1.28 ±.11	0.45 ±.07	0.17 ±.04	0.09 ±.03	0.02 ±.01	0.01 ±.01	

a. this table is based on 5232 trajectories

b. cross sections less than 0.005 a_0^2 are given as zero

Table 9
Energy transfer cross sections (in a_0^2) for the transitions from v = 6, j = 0 to the indicated final v', j' states at 0.5 eV relative translational energy.[a,b]

j' \ v'	0	1	2	3	4	5	6	7	all v'
0	0	0	0.01 ±.01	0.01 ±.01	0.01 ±.01	0.07 ±.04	...	0.02 ±.02	0.11 ±.05
2	0.04 ±.03	0.01 ±.01	0.01 ±.01	0.05 ±.02	0.09 ±.02	0.13 ±.05	12.60 ±.49	0.13 ±.05	13.06 ±.50
4	0.03 ±.01	0.05 ±.02	0.07 ±.03	0.07 ±.03	0.20 ±.04	0.40 ±.06	3.25 ±.20	0.10 ±.03	4.18 ±.22
6	0.08 ±.04	0.07 ±.02	0.15 ±.04	0.17 ±.04	0.21 ±.04	0.29 ±.05	1.00 ±.11	0.02 ±.01	2.01 ±.15
8	0.20 ±.05	0.14 ±.03	0.28 ±.05	0.24 ±.05	0.15 ±.04	0.15 ±.04	0.13 ±.03	0	1.29 ±.11
10	0.31 ±.06	0.18 ±.04	0.21 ±.05	0.14 ±.04	0.11 ±.03	0.11 ±.03	0.03 ±.02	0	1.09 ±.10
12	0.27 ±.06	0.09 ±.03	0.05 ±.02	0.04 ±.02	0.09 ±.03	0.08 ±.03	0		0.62 ±.09
14	0.03 ±.02	0.03 ±.01	0.03 ±.02	0.02 ±.01	0.02 ±.02	0			0.14 ±.04
16	0.04 ±.02	0.06 ±.03	0.05 ±.02	0.006 ±.005	0				0.16 ±.04
18	0.01 ±.01	0.03 ±.01	0.02 ±.01	0					0.06 ±.02
20	0	0.01 ±.01	0						0.02 ±.01
all j'	1.02 ±.12	0.67 ±.08	0.87 ±.09	0.76 ±.09	0.89 ±.09	1.23 ±.12	17.01 ±.54	0.27 ±.06	

a. this table is based in 3909 trajectories

b. cross sections less than 0.005 a_0^2 are given as zero

Table 10
Energy transfer cross sections (in a_0^2) for the transitions from v = 4, j = 6 to the indicated final v', j' states at 0.5 eV relative translational energy.[a,b]

j' \ v'	0	1	2	3	4	5	6	all v'
0	0.02 ±.02	0.01 ±.01	0.01 ±.01	0.02 ±.02	0.20 ±.04	0.01 ±.005	0	0.28 ±.05
2	0.03 ±.01	0.04 ±.02	0.04 ±.01	0.06 ±.01	0.78 ±.08	0.11 ±.02	0.007 ±.005	1.06 ±.09
4	0.11 ±.03	0.11 ±.03	0.11 ±.03	0.25 ±.06	3.31 ±.22	0.22 ±.06	0.009 ±.005	4.11 ±.24
6	0.09 ±.03	0.10 ±.03	0.11 ±.03	0.44 ±.08	...	0.11 ±.04	0	0.84 ±.10
8	0.10 ±.03	0.13 ±.03	0.20 ±.04	0.63 ±.01	2.26 ±.18	0.02 ±.02	0	3.33 ±.22
10	0.16 ±.04	0.25 ±.04	0.25 ±.04	0.33 ±.05	0.31 ±.05	0.006 ±.002	0	1.30 ±.09
12	0.21 ±.04	0.26 ±.04	0.20 ±.04	0.10 ±.03	0.02 ±.01	0	0	0.79 ±.08
14	0.18 ±.04	0.10 ±.02	0.10 ±.03	0.04 ±.02	0			0.43 ±.06
16	0.03 ±.01	0.02 ±.01	0.01 ±.01	0				0.07 ±.02
18	0.01 ±.01	0						0.01 ±.01
all j'	0.95 ±.09	1.02 ±.08	1.03 ±.08	1.88 ±.16	6.86 ±.48	0.47 ±.08	0.02 ±.01	

a. this table is based on 4061 trajectories

b. cross sections less than 0.005 a_0^2 are given as zero

Table 11
Energy transfer cross sections (in a_0^2) for the transitions from v = 2, j = 18 to the indicated final v',j' states at 0.5 eV relative translational energy.[a,b]

j' \ v'	0	1	2	3	4	5	6	7	all v'
0	0	0	0	0	0.01 ±.01	0	0	0	0.01 ±.01
2	0	0.02 ±.01	0.02 ±.01	0.006 ±.005	0.02 ±.01	0	0	0	0.06 ±.02
4	0.02 ±.02	0.02 ±.01	0.01 ±.01	0.02 ±.01	0.05 ±.02	0	0.01 ±.01	0	0.13 ±.03
6	0.04 ±.02	0.03 ±.01	0.02 ±.01	0.06 ±.02	0.05 ±.02	0.03 ±.02	0.01 ±.01	0	0.24 ±.05
8	0.04 ±.02	0.03 ±.01	0.04 ±.02	0.08 ±.03	0.05 ±.02	0.04 ±.02	0.04 ±.02	0.01 ±.01	0.32 ±.05
10	0.03 ±.02	0.03 ±.01	0.03 ±.01	0.05 ±.02	0.07 ±.02	0.05 ±.02	0.03 ±.01	0	0.29 ±.05
12	0.03 ±.02	0.04 ±.02	0.05 ±.02	0.06 ±.02	0.12 ±.03	0.10 ±.03	0.007 ±.005	0	0.39 ±.05
14	0.01 ±.01	0.03 ±.01	0.07 ±.02	0.39 ±.05	0.43 ±.06	0.05 ±.01	0		0.97 ±.08
16	0.07 ±.03	0.10 ±.04	0.48 ±.09	3.62 ±.24	0.23 ±.03	0			4.49 ±.27
18	0.05 ±.02	0.43 ±.09	...	0.15 ±.05	0				0.63 ±.10
20	0.47 ±.05	4.51 ±.27	0.12 ±.05	0	0				5.09 ±.28
22	0.67 ±.08	0.33 ±.04	0.006 ±.004	0					1.00 ±.09
24	0.06 ±.02	0	0						0.07 ±.02
all j'	1.49 ±.11	5.56 ±.29	0.84 ±.11	4.44 ±.26	1.02 ±.08	0.27 ±.04	0.09 ±.03	0.01 ±.01	

a. this table is based on 4506 trajectories

b. cross sections less than 0.005 a_0^2 are given as zero

Table 12
Energy transfer cross sections (in a_0^2) for the transitions from v = 0,j = 6 and v = 0,j = 18 states to the indicated final v',j' states at 0.5 eV relative translational energy.[a,b]

j' \ v'	v = 0,j = 6				v = 0,j = 18						
	0	1	2	all v'	0	1	2	3	4	5	all v'
0	0.09 ±.02	0.007 ±.003	0	0.10 ±.02	0	0	0	0	0	0	
2	0.43 ±.04	0.04 ±.01	0	0.47 ±.04	0.03 ±.02	0	0	0	0.01 ±.01	0	0.04 ±.02
4	1.69 ±.09	0.01 ±.01	0	1.70 ±.09	0.03 ±.02	0.04 ±.02	0.01 ±.01	0	0	0	0.09 ±.02
6	...	0.0	0		0.02 ±.01	0.04 ±.01	0.02 ±.01	0.01 ±.01	0.01 ±.01	0	0.10 ±.02
8	0.66 ±.06	0.0	0	0.66 ±.06	0.02 ±.01	0.06 ±.02	0.02 ±.01	0	0.01 ±.01	0	0.12 ±.03
10	0.02 ±.01	0.0	0	0.02 ±.01	0.02 ±.01	0.05 ±.02	0.04 ±.02	0.01 ±.01	0	0	0.13 ±.03
12	0	0	0		0.06 ±.02	0.08 ±.02	0.09 ±.02	0.03 ±.02	0		0.26 ±.04
14					0.13 ±.03	0.31 ±.04	0.28 ±.04	0.01 ±.01	0		0.74 ±.06
16					0.61 ±.09	2.66 ±.18	0.15 ±.02	0			3.41 ±.20
18					...	0.18 ±.05	0				0.18 ±.05
20					0.34 ±.07	0	0				0.34 ±.07
all j'	2.89 ±.18	0.05 ±.01	0		1.26 ±.12	3.42 ±.19	0.62 ±.06	0.07 ±.02	0.04 ±.02	0	

a. this table is based on 3835 trajectories for v = 0,j = 6 and 4097 for v = 0,j = 18

b. cross sections less than 0.005 a_0^2 are given as zero

is not reliable. The histogram cross sections converge well with respect to increasing the impact parameter even for adjacent-state transitions, and we think that they are more representative of the correct energy transfer cross sections. A method of presenting the data which is more appropriate to visual inspection is shown in Fig. 13. The matrices in Tables 8-12 were used with a computer contour program that generated contours by linear interpolation over triangles. Contours are spaced geometrically, being about a factor of three apart. The highest contour surrounds the initial state. It is clear that the "flow" of transition probability is a complicated function of the initial state. For the states with high j, the flow seems to be along lines of equal energy, *e.g.*, along a

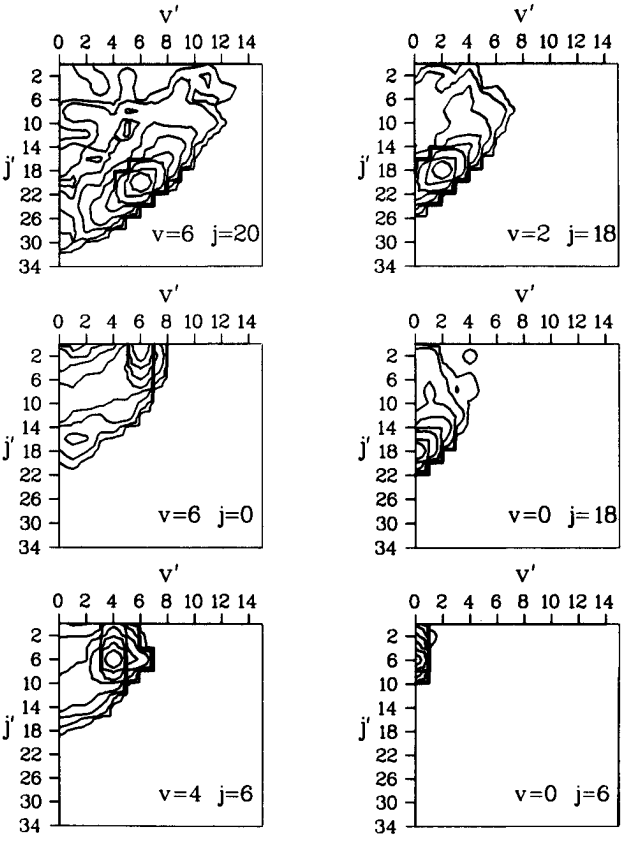

Fig. 13. Contour plots of equal cross section for molecular energy transfer, process (R1). Each plot is labeled by the initial state, and the axes indicate the final states. The relative translational energy is 0.5 eV and the contours have the values 9.0, 3.0, 1.0, 0.36, 0.12, 0.045, and 0.015 a_0^2. The contour of 9.0 a_0^2 is the one nearest to the initial molecular state.

diagonal line with a 45° positive slope in the figures. For low j most of the flow is along constant v' with v = 0,j = 6 being an extreme case. These patterns for the larger cross sections are similar to those observed in a recent trajectory study of He + H_2 collisions by Dove *et al.*[39] Transitions involving large changes in vibrational or rotational quantum number do not follow either of these major patterns.

Tables 8-12 show that the cross sections for energy transfer to states far removed from the initial state are reasonably large, so that large-Δv or large-Δj transitions are not unlikely in H + H_2 collisions. We also reported vibrational transitions with large quantum number changes for Ar + H_2 at a collision temperature of 4500 K;[40,41] in that study the initial rotational state of H_2 was averaged over a thermal distribution at 4500 K, and the rate constants were summed over final rotational states.* Seven of the eight distorted wave-type theoretical modesl we tested against the 4500 K data for Ar + H_2 badly underestimated the multiple-quantum transitions by comparison to the trajectory results.[41]

We hope that Tables 8-12 will be useful in showing the systematics of molecular energy transfer and will facilitate obtaining a reasonable functional form for representing $\sigma(v,j \to v',j')$ over a wide range of Δv and Δj. There have been some important developments recently in energy scaling theories to treat transitions of the kind we observe here;[42,43] but the theory as developed so far is not applicable to our data because it requires a set of de-excitation cross sections at the same initial kinetic energy.

For two of the initial states included in Fig. 13, namely v = 2,j = 18 and v = 6,j = 0, we also present energy transfer results in Fig. 14. The final state distributions for non-exchange collisions are compared to those for reactive, or exchange, collisions. For the non-exchange collisions, the cross sections were computed by a combination of histogramming and smooth sampling, as we did for Fig. 13. For the exchange cross sections, we used only smooth sampling. All of the plots in Fig. 14 have the same contour values. Clearly, the pattern of final states differs considerably for the two pathways. For the non-exchange collisions, those states immediately adjacent to the initial state always have the largest cross sections. In contrast, for exchange products, states far removed

*Some preliminary results for a fixed E_{rel} are published in reference 12, but much more extensive fixed-energy calculations for the six initial states considered here were completed subsequently and are still undergoing analysis.

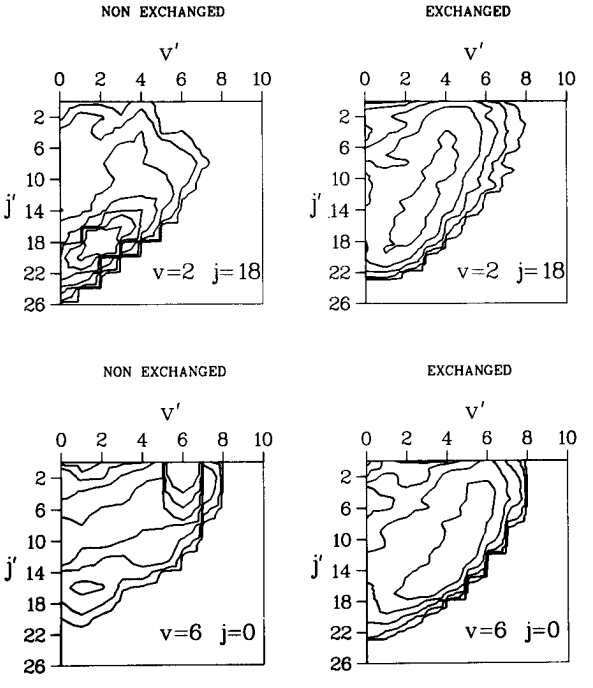

Fig. 14. Contour plots of equal cross sections for the state-to-state processes (R1) and (R2). The relative translational energy is 0.5 eV and the contours have the values 3.75, 1.25, 0.417, 0.139, 0.046, 0.015, and 0.005 a_0^2. The innermost contours have the largest value and the values diminish monotonically (within statistical error) to the edges.

from the initial state have cross sections as large as the initial state has; in fact, for $v = 6, j = 0$ the final state of $v' = 4, j' = 14$ has a larger cross section than the $v' = 6, j' = 0$ state. Also, the density of contours shows that the cross section distribution has a different shape for the two mechanisms, (R1) and (R2), in particular. Therefore, the probability of multiple quantum transitions is even higher if the collision leads to exchange than it is for nonreactive products. Incidentally, the largest cross section for a transition from the $v = 0, j = 6$ state corresponds to an internal energy gain, while the state at the far end of the most probable contour from $v = 2, j = 18$ corresponds to an internal energy loss.

Table 13
Cross sections (in a_0^2) for producing specified final states from $H_2(v=0,j=2)$ by processes (R1) and (R2).

v'	j'	nonreactive	reactive
	T = 444 K		
0	0	1.3 ± 0.2(-2)	3.7 ± 1.7(-5)
	1	0	2.7 ± 0.8(-4)
	2	...	2.0 ± 0.5(-4)
	3	0	9.7 ± 2.9(-5)
	4	2.5 ± 0.4(-3)	8.5 ± 5.2(-6)
	T = 875 K		
0	0	1.2 ± 0.2(-1)	6.8 ± 4.8(-3)
	1	0	2.2 ± 0.9(-2)
	2	...	1.4 ± 0.4(-2)
	3	0	8.8 ± 3.4(-3)
	4	8.5 ± 1.0(-2)	3.3 ± 1.4(-3)
	5	0	3.0 ± 1.1(-3)
	6	2.0 ± 0.5(-3)	6.8 ± 3.0(-4)
	T = 1000 K		
0	0	2.6 ± 0.4(-1)	9.0 ± 5.0(-3)
	1	0	1.8 ± 0.6(-2)
	2	...	2.1 ± 0.7(-2)
	3	0	2.4 ± 0.8(-2)
	4	1.2 ± 0.2(-1)	1.2 ± 0.5(-2)
	5	0	6.5 ± 2.5(-3)
	6	4.5 ± 2.2(-3)	5.5 ± 2.4(-3)
	T = 2400 K		
0	0	5.7 ± 2.6(-1)	1.5 ± 1.4(-2)
	1	0	4.3 ± 2.6(-1)
	2	...	1.2 ± 0.6(-1)
	3	0	7.7 ± 2.9(-2)
	4	1.3 ± 0.3	1.6 ± 0.6(-1)
	5	0	9.2 ± 3.5(-2)
	6	1.7 ± 0.5(-1)	5.4 ± 2.2(-2)
	7	0	1.1 ± 0.3(-1)
	8	4.2 ± 1.0(-2)	7.7 ± 2.8(-2)
	9	0	3.8 ± 1.1(-2)
	10	6.3 ± 2.2(-3)	3.7 ± 0.8(-2)
	11	0	8.9 ± 2.0(-3)
	12	2.8 ± 1.5(-3)	6.0 ± 1.2(-3)
	13	0	1.5 ± 0.5(-3)
1	0	1.4 ± 0.9(-3)	small
	1	0	1.1 ± 0.8(-2)
	2	7.8 ± 3.2(-3)	2.9 ± 1.4(-3)
	3	0	1.1 ± 0.6(-2)
	4	1.3 ± 0.5(-2)	1.2 ± 0.5(-2)
	5	0	7.3 ± 3.8(-3)
	6	1.3 ± 0.7(-2)	3.9 ± 1.6(-3)
	7	0	2.6 ± 1.0(-3)
	8	small	3.2 ± 1.2(-3)
	9	0	1.6 ± 0.8(-3)

We can also compare the energy transfer cross sections for nonreactive collisions to those for reactive collisions when both are averaged over distributions of relative translational energy. This is done for the v = 0,j = 2 state in Table 13. The cross sections in this table are all calculated by the histogram method, and they are averaged over thermal distributions of relative translational energy at four different temperatures. The cross sections for nonreactive energy transfer are larger than those for reactive energy transfer. Excitations through the reactive path become relatively more competitive at higher temperatures for this initial state.

VII. DISSOCIATION

We previously reported collision-induced dissociation cross sections for Ar + H_2 collisions for 22 initial states with a total energy 1.0 eV greater than the energetic threshold (E_{tot} = 1.0 eV).[12,44] For comparison we have calculated dissociation cross sections for H + H_2 collisions for 8 of these initial states, again at E_{tot} = 1.0 eV. The states chosen are in each case the highest-energy or second-highest energy even-j state for a given v. Thus, all have internal energies within 0.39 eV of the dissociation limit. The comparison for these states is given in Fig. 15 and Table 14 (Table 14 also contains one lower-energy state, the 4,0 state). Figure 15 compares the data to cross sections calculated from the line-of-centers (LOC) model:[44]

$$\sigma^{LOC}(v,j,E_{rel}) = \sigma_h(v,j,E_{rel})\,\theta(E_{rel} - D_{v,j})\left(1 - \frac{D_{v,j}}{E_{rel}}\right) \tag{9}$$

where $D_{v,j}$ is the energy required to dissociate the state v,j, $\theta(x)$ is the Heaviside function, and $\sigma_h(v,j,E_{rel})$ is the hard-sphere cross section. For the latter we used

$$\sigma_h(v,j,E_{rel}) = \pi[D_{12}(v,j,E_{rel})]^2 \tag{10}$$

where the hard-sphere radius for state v,j was approximated by

$$D_{12}(v,j,E_{rel}) = R_0(E_{rel})\,\frac{\langle r^2\rangle^{1/2}_{v,j}}{\langle r^2\rangle^{1/2}_{0,0}} \tag{11}$$

In this expression $\langle r^2\rangle^{1/2}_{v,j}$ is the root-mean-square value[45] of the H_2 internuclear distance r in state v,j, and $R_0(E_{rel})$ is the solution of

$$V_0(r_e,R_0) = E_{rel} \tag{12}$$

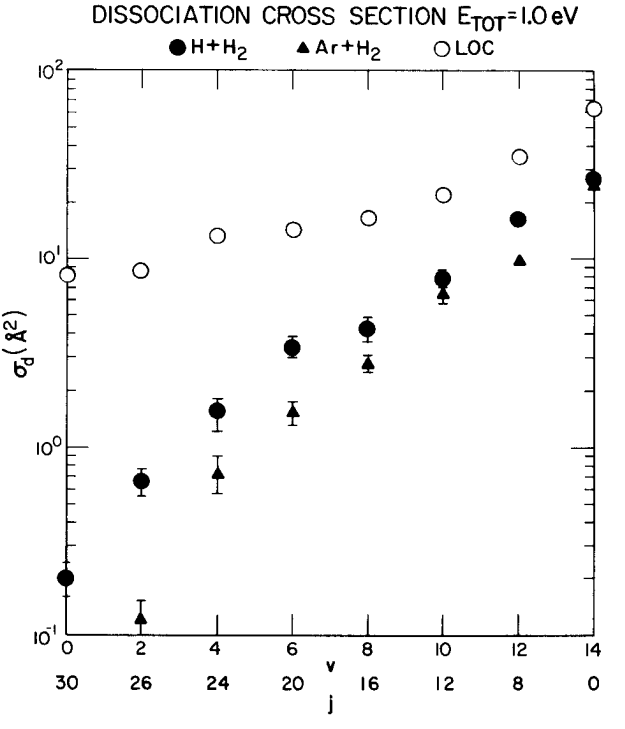

Fig. 15. The dissociation cross section (in Å^2) plotted against the initial molecular state quantum numbers. All the states have approximately the same internal energy. Three sets of points are plotted: filled circles correspond to H + H_2, filled triangles to Ar + H_2, and open circles are values calculated from a line-of-centers (LOC) model.

where $V_0(r,R)$ is the spherical average[1] of the H-H_2 interaction potential for an H-H distance of r and an H-to-center-of-mass-of-H_2 distance R. The LOC model has been a popular model to use to estimate dissociation cross sections, but it is clearly inappropriate in the present case as well as for Ar + H_2. Figure 15 shows that for initial states with low v and high j, the hydrogen atom is a much more effective dissociator than is Ar. Yet at high v and low j they are nearly equally effective, despite the fact that the relative translational energies for all of the cases in Fig. 15 are in the range 1.02-1.39 eV. Part of the reason may lie in the differences between the potential surfaces; this could be tested by additional runs in which only the mass was changed. Alternatively we can use the Massey parameter[46] to rationalize the observed results in terms of the difference between the H_2 oscillator period and the collision time. The oscillator period for H_2 in the v = 0, j = 30 state is 0.015 ps, which is about the same as the collision time for an H + H_2 collision, 0.010 to 0.015 ps. An Ar + H_2 collision occurs in about

Table 14
The cross sections (in $\mathring{A}^2$) for dissociation of H_2 by collisions with H atoms or with Ar atoms. The total energy is 1.0 eV in excess of the energy required for dissociation.

v,j state	N[a]	H atoms	Ar atoms
0,30	1778	0.20 ± .04	0.000 ± .005
2,26	1000	0.66 ± .11	0.12 ± .03
4,0	1000	0.11 ± .05	0.01 ± .01
4,24	1000	1.56 ± .24	0.73 ± .18
6,20	1000	3.41 ± .37	1.53 ± .21
8,16	1000	4.23 ± .60	2.73 ± .27
10,12	1000	7.92 ± .71	6.50 ± .69
12,8	1000	16.2 ± 0.9	9.72 ± .50
14,0	1000	26.4 ± 1.1	25.4 ± 0.7

a. number of trajectories for H-atom case

0.02 to 0.03 ps, assuming a similar range of forces. The Massey parameter suggests that the H atom should be more effective in causing energy transfer and hence dissociation. A hydrogen molecule in the $v = 14, j = 0$ state has a period of 0.089 ps, much longer than the collision time for either H atoms or Ar atoms, so that both should be very effective. However, it is doubtful if the great disparity in the cross section between H atoms and Ar atoms, at least a factor of 40 at $v = 0, j = 30$, can be accounted for solely by this kind of argument.

Further details of these calculations, including cross sections for production of quasibound states and dissociation cross sections averaged over a thermal distribution of relative translational energy, will be published elsewhere.

VIII. SUMMARY

An extensive set of quasiclassical trajectory calculations has been made for the $H + H_2$ system using the most accurate potential energy surface available, the LSTH potential, to describe the interatomic forces. Several runs were made at low collision energies and with low-energy initial states of H_2 to compare with other reported work, both quantum mechanical and classical. In general, reasonably good agreement with quantal results was found where it could be expected. Our results also agreed well with the other quasiclassical work. In the comparison with the quantal rigid-rotator calculations, there appears to be a partial cancellation of errors between the rigid-rotator assumption in the quantal calculations and the threshold errors in the trajectory calculations.

Thermal rate constants and activation energies for the exchange reaction were calculated at three temperatures, 444, 875, and 2400 K. Where reliable experimental results are available, the results compared very favorably. The transition state results and our trajectory results also agree well with each other.

A major effort was made to describe the reactivity and energy transfer characteristics of the H_3 system for the higher-internal-energy states of the H_2 molecule. Several important attributes of the reactive scattering, namely activation energy, average final vibrational quantum number, average final rotational quantum number, and scattering angle, were obtained for many (28) initial states spanning the entire range of bound states of para-H_2. These calculations were all for a relative translational temperature of 300 K. Energy transfer cross sections for nonreactive transitions at a relative translational energy of 0.5 eV from six initial v,j states to all of the dynamically allowed final states were also obtained, in many cases with good statistical accuracy. In the reactive cases we found a tendency for vibrational adiabaticity and $R \rightarrow T$ energy transfer, except at low j where rotational adiabaticity and $V \rightarrow R$ energy transfer could be observed; in nonreactive cases we found a tendency to conserve internal energy although the overall trends including small-transition-probability processes are more complicated. In the reactive cases, we found that vibration and rotation both promote reaction, decrease the activation energy, and lower the average molecular scattering angle, but vibration is more effective in the first two respects and rotation in the third.

The dissociation characteristics of $H + H_2$ were also studied briefly and compared to previous work on $Ar + H_2$. Hydrogen atoms were found to be more effective than Ar atoms in dissociation, quite dramatically so for some states.

IX. ACKNOWLEDGMENTS

This work was performed under the auspices of the U.S. Department of Energy and was also supported in part by the National Science Foundation.

X. REFERENCES

1. D. G. Truhlar and C. J. Horowitz, Functional representation of Liu and Siegbahn's accurate *ab initio* potential energy calculations for H + H_2, J. Chem. Phys. 68: 2466 (1978); 71: 1514(E) (1979).
2. B. Liu, *Ab initio* potential energy surface for linear H_3, J. Chem. Phys. 58: 1925 (1973).
3. P. Siegbahn and B. Liu, An accurate three-dimensional potential energy surface for H_3, J. Chem. Phys. 68: 2457 (1978).
4. D. G. Truhlar and R. E. Wyatt, History of H_3 kinetics, Annu. Rev. Phys. Chem. 27: 1 (1976).
5. D. G. Truhlar and R. E. Wyatt, H + H_2: Potential energy surfaces and elastic and inelastic scattering, Advan. Chem. Phys. 36: 141 (1977).
6. R. B. Walker, E. B. Stechel, and J. C. Light, Accurate H_3 dynamics on an accurate H_3 potential surface, J. Chem. Phys. 69: 2922 (1978).
7. S. Green and D. G. Truhlar, Rotational excitation of hydrogen molecules by collisions with hydrogen atoms, Astrophys. J. 231: L101 (1979).
8. R. I. Altkorn and G. C. Schatz, A new method for determining semiclassical tunneling probabilities in atom-diatom reactions, J. Chem. Phys. 72: 3337 (1980).
9. H. R. Mayne and J. Toennies, Quasiclassical cross sections for the H + $H_2(0,0) \rightarrow$ H + H_2 reaction: Comparison of the Siegbahn-Liu-Truhlar-Horowitz and the Porter-Karplus potential surfaces, J. Chem. Phys. 70: 5314 (1979).
10. H. R. Mayne, Quasiclassical trajectory calculations for H + H_2(v=1) on a new potential energy surface, Chem. Phys. Lett. 66: 487 (1979).
11. W. Kolos and L. Wolniewicz, Potential energy curves for the $X\ ^1\Sigma_g^+$, $b\ ^3\Sigma_g^+$, and the $C\ ^1\Pi_u$ states of the hydrogen molecule, J. Chem. Phys. 43: 2429 (1965).
12. N. C. Blais and D. G. Truhlar, Monte Carlo trajectory study of Ar + H_2 collisions. I. Potential energy surface and cross sections for dissociation, recombination, and inelastic scattering, J. Chem. Phys. 65: 5335 (1976).
13. D. L. Bunker and N. C. Blais, Monte Carlo calculations. V. Three-dimensional study of a general bimolecular interaction potential, J. Chem. Phys. 41: 2377 (1964).

14. M. Karplus, R. N. Porter, and R. D. Sharma, Exchange reactions with activation energy. I. Simple barrier potential for (H,H_2), J. Chem. Phys. 43: 3259 (1965).
15. J. T. Muckerman and M. B. Faist, Rate constants from Monte Carlo quasiclassical trajectory calculations. A procedure for importance sampling, J. Phys. Chem. 83: 79 (1979).
16. N. C. Blais and D. G. Truhlar, Monte Carlo trajectory study of $Ar + H_2$: Vibrational selectivity of dissociative collisions at 4500 K and the characteristics of dissociation under equilibrium conditions, J. Chem. Phys. 70: 2962 (1979).
17. R. C. Tolman, "Statistical Mechanics with Applications to Physics and Chemistry", Chemical Catalog Co., New York (1927), pp. 266-270.
18. D. G. Truhlar, Interpretation of the activation energy, J. Chem. Educ. 55: 309 (1978).
19. D. G. Truhlar and J. T. Muckerman, Reactive scattering cross sections III: Quasiclassical and semiclassical methods, in: "Atom-Molecule Collision Theory: A Guide for the Experimentalist", R. B. Bernstein, ed., Plenum, New York (1979), p. 505.
20. R. B. Walker, E. B. Stechel, and J. C. Light, unpublished; R. B. Walker, personal communication.
21. R. B. Walker and E. B. Stechel, unpublished results quoted in reference 7.
22. B. C. Garrett and D. G. Truhlar, unpublished.
23. B. C. Garrett and D. G. Truhlar, Reliable *ab initio* calculation of a chemical reaction rate and a kinetic isotope effect: $H + H_2$ and $D + D_2$, Proc. Natl. Acad. Sci. USA 76: 4755 (1979).
24. W. R. Schulz and D. J. LeRoy, Kinetics of the reaction $H + p\text{-}H_2 \rightarrow o\text{-}H_2 + H$, J. Chem. Phys. 42: 3869 (1965).
25. K. A. Quickert and D. J. LeRoy, Test of transition-state theory using the experimentally determined rate constant ratio for the reactions $H + H_2$ and $H + D_2$, J. Chem. Phys. 53: 1325 (1970); 54: 5444(E) (1971).
26. A. A. Westenberg and N. deHaas, Atom-molecule kinetics using ESR detection. II. Results for $D + H_2 \rightarrow HD + H$ and $H + D_2 \rightarrow HD + D$, J. Chem. Phys. 47: 1393 (1967).
27. A. Farkas, Über die thermische Parawasserstoffwandlung, Z. Phys. Chem. B 10: 419 (1930).
28. H. van Meersche, Contribution à l'étude de la cinetique des reactions entre l'hydrogene atomique et l'hydrogene moleculaire, Bull. Soc. Chim. Belg. 60: 99 (1951).
29. B. C. Garrett and D. G. Truhlar, Generalized transition state theory. Classical mechanical theory and applications to collinear reactions of hydrogen molecules, J. Phys. Chem. 83: 1052 (1979); 83: 3058(E) (1979).
30. B. C. Garrett and D. G. Truhlar, Improved treatment of threshold contributions in variational transition-state theory, J. Phys. Chem. 84: 1730 (1980).

31. D. G. Truhlar and A. Kuppermann, Exact and approximate quantum mechanical reaction probabilities and rate contants for the collinear H + H_2 reaction, J. Chem. Phys. 56: 2232 (1972).
32. D. G. Truhlar and J. C. Gray, Interpretation and temperature dependence of the energy of activation for the reactions H + Cl_2, H_2 + I, H + H_2, and isotopic analogs, Chem. Phys. Lett. 57: 93 (1978).
33. J. C. Gray, D. G. Truhlar, and M. Baer, Test of trajectory calculations against quantum mechanical state-to-state and thermal collinear reaction rates for H + Cl_2, J. Phys. Chem. 83: 1045 (1979).
34. N. C. Blais, D. G. Truhlar, and B. C. Garrett, Dynamical calculation of the temperature dependence of the activation energy for a chemical reaction from 444 K to 2400 K, J. Phys. Chem., to be published.
35. B. A. Blackwell, J. C. Polanyi, and J. J. Sloan, Effect of changing reagent energy on reaction dynamics. VIII. Highly vibrationally-excited product from the thermoneutral reaction Cl + OH($v \leq 9$) → HCl($v' \leq 11$) + O, Chem. Phys. 24: 25 (1977).
36. D. G. Truhlar and D. A. Dixon, Direct mode chemical reactions II: Classical theories, in: "Atom-Molecule Collision Theory: A Guide for the Experimentalist", R. B. Bernstein, ed., Plenum, New York (1979), p. 595.
37. J. C. Polanyi, Molecular beam scattering, Faraday Disc. Chem. Soc. 55: 389 (1973).
38. J. W. Duff and D. G. Truhlar, Tests of semiclassical treatments of vibrational-translational energy transfer in collinear collisions of helium with hydrogen molecules, Chem. Phys. 9: 243 (1975).
39. J. E. Dove, S. Raynor, and H. Teitelbaum, A quasiclassical trajectory study of molecular energy transfer in H_2-He collisions, Chem. Phys. 50: 175 (1980).
40. N. C. Blais and D. G. Truhlar, Monte Carlo trajectory study of Ar + H_2 collisions, Translation to vibration energy transfer from different initial states, in: "State-to-State Chemistry", P. R. Brooks and E. F. Hayes, eds., American Chemical Society, Washington, D.C. (1977), p. 243.
41. J. W. Duff, N. C. Blais, and D. G. Truhlar, Monte Carlo trajectory study of Ar + H_2 collisions: Thermally averaged vibrational transition rates at 4500 K, J. Chem. Phys. 71: 4304 (1979).
42. A. E. DePristo, S. D. Augustin, R. Ramaswamy, and H. Rabitz, Quantum number and energy scaling for nonreactive collisions, J. Chem. Phys. 71: 850 (1979).
43. A. E. DePristo and H. Rabitz, A scaling theoretical analysis of vibrational relaxation experiments: Rotational effects and long-range collisions, Chem. Phys. 44: 171 (1979).

44. N. C. Blais and D. G. Truhlar, Monte Carlo trajectory study of Ar + H_2 collisions. II. Vibrational and rotational enhancement of cross sections for dissociation, J. Chem. Phys. 66: 772 (1977).
45. R. J. LeRoy, Eigenvalues and certain expectation values for all bound and quasibound levels of ground-state ($X\ ^1\Sigma_g^+$) H_2, HD, and D_2, technical report WIS-TCI-387, University of Wisconsin, Madison, 1971.
46. M. S. Child, "Molecular Collision Theory", Academic, London (1974).